

Online Auto-Tuning Method in Field-Orientation-Controlled Induction Motor Driving Inertial Load

MASAKI NAGATAKI¹ (Member, IEEE), KEIICHIRO KONDO¹ (Member, IEEE), OSAMU YAMAZAKI², KAZUAKI YUKI², AND YOSUKE NAKAZAWA²

¹School of Advanced Science and Engineering, the Department of Electrical Engineering and Bio-science, Waseda University, Shinjuku 1698555, Japan

²Toshiba Infrastructure Systems & Solutions Corporation, Fuchu 1838511, Japan

CORRESPONDING AUTHOR: MASAKI NAGATAKI (e-mail: mnagataki@ruri.waseda.jp)

This work was supported by Toshiba Infrastructure Systems and Solutions Corporation.

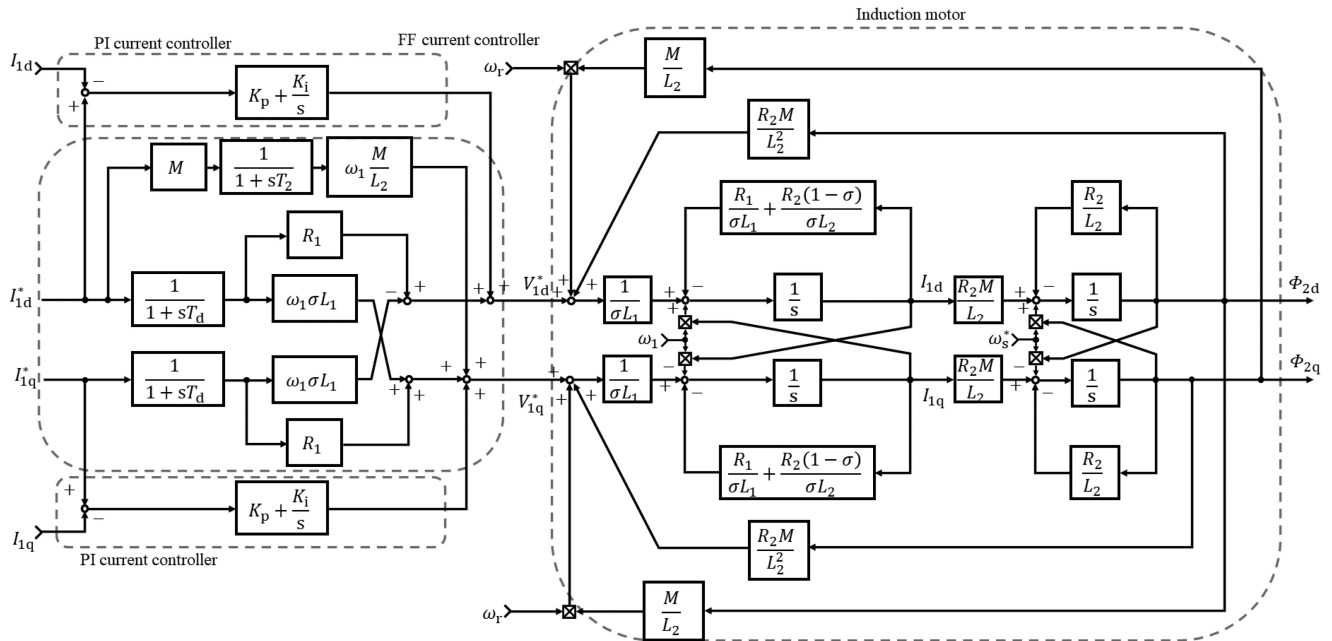
ABSTRACT Feed-forward current control, which employs a single-pulse mode of inverters over a wide speed range, is applied in inertial load drive applications such as electric vehicles and electric railway vehicles. It is necessary to identify both primary and secondary motor parameters to realize sophisticated torque control in the feed-forward current control region, wherein the current controller cannot compensate for motor parameter errors. An online auto-tuning method that is based on the fundamental components of motor voltages during acceleration with an inertial load is proposed in this study. The convergence of the proposed auto-tuning is discussed, and a calculation method for correction gains is proposed to compensate for the motor parameters. The proposed method is verified via numerical simulation and experiments with a 750 W induction motor and an inertial load.

INDEX TERMS Induction motors, motor drives, parameter estimation, variable speed drives.

I. INTRODUCTION

The field-orientation-controlled induction motor is widely employed for inertial load-drive applications such as electric vehicles and electric railway vehicles that require a high torque performance over a wide speed range [1]. Fig. 1 shows the field-orientation-control (FOC) system of an induction motor (IM). The currents and voltages illustrated in Fig. 1 are presented in a rotating d- and q-axis reference frame with a primary angular frequency. The current controller is composed of a feed-forward (FF) and the feedback (FB) proportional-integral (PI) current controllers; the former calculates the voltage commands based on the induction motor parameters and current commands, and the latter compensates for the motor parameter errors and the transient response of the current. In the indirect FOC (IFOC), the phase angle of the secondary flux is controlled by an appropriate slip angular frequency command that enables independent control of excitation and torque currents in terms of the rotor angular frequency [2]. The misalignment of the secondary flux with respect to the d-axis occurs when the current controller has

motor parameter errors; this degrades the accuracy of torque control. In FOCs for high-power applications such as electric railway vehicle drives, FF current control, which includes single-pulse control of the inverter, is employed to minimize the switching loss over a wide speed range [3], [4]. The current control mode is switched from the PI current control that the sufficient voltage margin is needed for the current control to the FF current control when the modulation ratio is reached to the over modulation region. The pulse mode is switched from the multi-pulse pulse-width-modulation (PWM) mode to the single-pulse control mode when the motor voltage is reached to the maximum of the inverter output voltage. The switching control mode, desired voltage, and torque control do not continue seamlessly in the high-speed region when the current controller has motor parameter errors because the current controller cannot compensate for motor parameter errors by the PI control in the FF current control region, as shown in Fig. 2. Thus, it is essential to identify both the primary and secondary motor parameters for realizing a high torque control performance.



R_1 : primary resistor, R_2 : secondary resistor, L_1 : primary self-inductance, L_2 : secondary self-inductance, M : mutual inductance, $\sigma = 1 - \frac{M^2}{L_1 L_2}$: leakage coefficient, σL_1 : primary leakage inductance in FOC, ω_r : secondary angular frequency, ω_s^* : slip angular frequency command, ω_1 : primary angular frequency, $T_2 = \frac{L_2}{R_2}$: secondary time constant, I_{1d} : d-axis current, I_{1d}^* : d-axis current command, I_{1q} : q-axis current, I_{1q}^* : q-axis current command, V_{1d}^* : d-axis voltage command, V_{1q}^* : q-axis voltage command, T_d : time constant of current regulator, K_p : proportional gain, K_i : integral gain

FIGURE 1. Configuration of FOC system of IM.

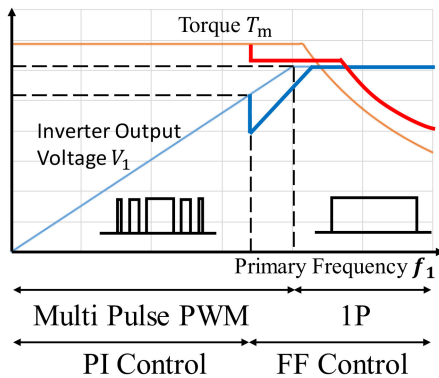


FIGURE 2. Torque and inverter output voltage.

This study aims to propose an online auto-tuning method with an inertial load that can identify the primary and secondary motor parameters. This study is aimed at inertial load-drive applications. A low-computational-load tuning method is desirable because the computational capacity of the controller in the inertial load-drive applications is not high; this method can identify motor parameters based on the fundamental frequency component of the motor voltage or current during acceleration operation. However, it is difficult to identify motor parameters from the motor voltage or current, and this corresponds to solving the state equations of the induction motor [5–7]. One solution is applying an observer [8], [9]

or least mean square (LMS) methods [10]–[18]. Although these methods are applicable to online auto-tuning for inertial load-drive applications, they require a high computational capacity controller. Other solutions include methods used for identifying motor parameters based on the step [19]–[22] or frequency responses [23]–[29]. References [19] and [20] present a method to adjust the secondary time constant of the IM based on the transient response of the d- and q-axis voltages when the step signal of the q-axis current is input. In this method, the IM is rotated at a constant speed using a load motor. Reference [21] shows the method to identify the secondary time constant of the IM according to the motor current and voltage when the step signal of the motor rotational speed is inputted by the load motor. Reference [22] presented a method for identifying the magnetizing curve of the primary self-inductance of an IM based on the transient response of the motor voltage when the step signal of the d-axis current is input at standstill. These methods [19]–[22] focus on the information of the flux included in the motor voltage during the transient response, and therefore, they require a load motor or additional signal. The methods in [23]–[27] identify motor parameters based on the frequency response when an AC signal is superimposed on the motor voltage. Reference [28] presented a method for identifying motor parameters by inputting a high-frequency voltage to the motor without rotation. Another method that measures the motor impedance characteristics and identifies the magnetizing curve has been

proposed [29]. The methods in [23]–[29] focus on the frequency characteristics of the IM and require the injection of an additional high-frequency signal. Thus, previous conventional studies are not suitable for online auto-tuning methods in inertial load-drive applications. The methods in [8]–[18] are not applicable to inertial load-drive applications because they require a high computational capacity. The methods in [19]–[21] require load control, and therefore, these methods are not applicable to the inertial load-drive applications. The methods in [23]–[29] require a frequency analyzer, high-computational-capacity controller, or additional signals that influence the motor torque; thus, these methods are not suitable for online auto-tuning.

In the inertial load drive, the motor speed changes gradually, such that the PI current controller voltage is proportional to the primary angular frequency and motor parameter errors. Therefore, the derivative of the PI current controller voltage of the primary angular frequency is proportional to the motor parameter error. In [30], we proposed an auto-tuning method that use the features of an inertial load drive. The motor voltage is a function of current, flux and frequency; therefore, the inductance can be estimated by changing the flux or frequency. Given this context, the method proposed in this study is categorized as a method for estimating the parameters by changing the frequency or motor speed. The ratio of the motor voltage to the primary angular frequency is equivalent to the primary linkage flux in the high-speed region; the voltage drop of the primary resistance is negligible. Information on the leakage and secondary fluxes is included in the ratio of the output voltage of the PI current controller to the primary angular frequency. Therefore, in the proposed method, the primary self-inductance is adjusted based on the motor voltage that is proportional to the primary linkage flux in the high-speed region. Then, the primary leakage inductance in FOC and secondary time constant are adjusted based on the ratio of the output voltage of the PI current controller to the primary angular frequency during the acceleration operation. Finally, the primary resistance is adjusted based on the output voltage of the PI current controller during acceleration. This method can identify both the primary and secondary motor parameters according to only the fundamental component of the motor voltage during acceleration with an inertial load. Since the motor voltage during acceleration changes gradually in inertial load-drive applications, this method can make the sampling frequency of the auto-tuning controller much lower, for instance 100 Hz, and it can be applied to online auto-tuning for inertial load-drive applications. The proposed method requires a lower computational capacity compared with [8]–[18], does not need a load motor compared with [19]–[22], and uses only the fundamental components of the motor voltages compared with [23]–[29].

However, the convergence of the auto-tuning method was not revealed in [30]. The calculation methods for the correction gains to adjust the motor parameters have also not been

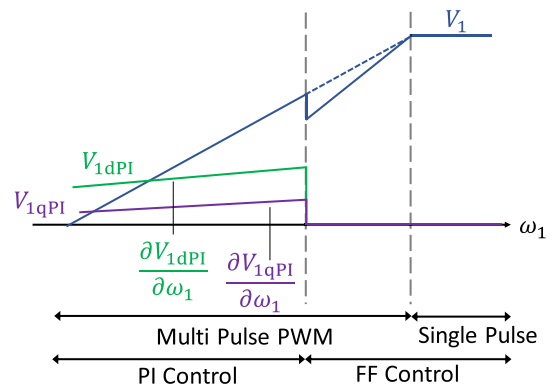


FIGURE 3. Output voltage of inverter and PI controller.

clarified. The proposed auto-tuning method does not converge or takes a long time to converge when the correction gains are inappropriate. Therefore, the calculation methods are required for the correction gains in which the auto-tuning converges fewer times. In this study, the proposed method for determining the correction gains based on the mathematical model of the IM is presented.

The remainder of this manuscript is organized as follows: Section II reveals the relationship between the output voltage of the PI current controller and motor parameter errors; further, the proposed auto-tuning method is described. The calculation method for the correction gains and convergence of the proposed auto-tuning method are presented in Section III. The simulation and experimental results are respectively presented in Sections IV and V. Finally, Section VI concludes the paper.

II. THEORY OF PROPOSED AUTO-TUNING METHOD

Fig. 3 shows the output voltage of the inverter and PI current controller with respect to the primary angular frequency when the current controller has motor parameter errors. The broken line in Fig. 3 represents the output voltage of the inverter without motor-parameter errors. The PI current controller outputs the voltage to compensate for the motor parameter errors. The output voltage of the PI current controller has a primary angular frequency dependency because the error of the electromotive force is proportional to the primary angular frequency in the steady state during acceleration operation. The relationship between the output voltage of the PI current controller and motor parameter errors in the steady state is analyzed by assuming that the d- and q-axis currents are constant in the PI current control region.

A. CONFIGURATION OF CURRENT CONTROLLER

The voltage equations of the IM represented in a rotating d- and q-axis reference frame with the primary angular

frequency are presented as

$$\begin{bmatrix} V_{1d} \\ V_{1q} \\ 0 \\ 0 \end{bmatrix} = \begin{bmatrix} R_1 + p\sigma L_1 & -\omega_1\sigma L_1 & p\left(\frac{M}{L_2}\right) & -\omega_1\left(\frac{M}{L_2}\right) \\ \omega_1\sigma L_1 & R_1 + p\sigma L_1 & \omega_1\left(\frac{M}{L_2}\right) & p\left(\frac{M}{L_2}\right) \\ -R_2\left(\frac{M}{L_2}\right) & 0 & p + \frac{R_2}{L_2} & -\omega_s^* \\ 0 & -R_2\left(\frac{M}{L_2}\right) & \omega_s^* & p + \frac{R_2}{L_2} \end{bmatrix} \times \begin{bmatrix} I_{1d} \\ I_{1q} \\ \Phi_{2d} \\ \Phi_{2q} \end{bmatrix} \quad (1)$$

The slip angular frequency command ω_s^* is given by

$$\omega_s^* = K_s \frac{I_{1q}^*}{I_{1d}^*} \quad (2)$$

where the slip gain K_s represents the reciprocal of the secondary time constant of the IM; the true value of the slip gain K_s is R_2/L_2 . A misalignment of the secondary flux occurs when the slip gain contains errors. When the q-axis secondary flux is zero, the d- and q-axis voltages V_{1d} and V_{1q} in the steady state are respectively expressed as

$$V_{1d} = R_1 I_{1d} - \omega_1 \sigma L_1 I_{1q} \quad (3)$$

$$V_{1q} = R_1 I_{1q} + \omega_1 \sigma L_1 I_{1d} + \omega_1 \frac{M}{L_2} \Phi_{2d} \quad (4)$$

When the IFOC is realized, the primary leakage inductance σL_1 and the d-axis secondary flux Φ_{2d} in (3) and (4) are given by

$$\sigma L_1 = L_1 - \frac{M^2}{L_2} \quad (5)$$

$$\Phi_{2d} = M I_{1d} \quad (6)$$

Given this context, the FF current controller voltages V_{1dFF} and V_{1qFF} are respectively expressed as

$$V_{1dFF} = R_1 \frac{1}{1 + sT_d} I_{1d}^* - \omega_1 \sigma L_1 \frac{1}{1 + sT_d} I_{1q}^* \quad (7)$$

$$V_{1qFF} = R_1 \frac{1}{1 + sT_d} I_{1q}^* + \omega_1 \sigma L_1 \frac{1}{1 + sT_d} I_{1d}^* + \omega_1 \frac{M^2}{L_2} \frac{1}{1 + sT_2} I_{1d}^* \quad (8)$$

where $1/(1 + sT_d)$ and $1/(1 + sT_2)$ are the first order delay controllers to imitate the responses of the current and flux. Although the voltage drop terms are generally not included in (7) and (8) in IFOC, the voltage drop terms are needed to compensate for the motor voltage in the FF current control region for inertial load-drive applications such as electric railway vehicles as shown in Fig. 2. The PI controller is assumed as the FB controller in this study; the d- and q-axis output voltage commands V_{1d}^* and V_{1q}^* are respectively expressed as

$$V_{1d}^* = \left(K_p + \frac{K_i}{s} \right) (I_{1d}^* - I_{1d}) + R_1 \frac{1}{1 + sT_d} I_{1d}^*$$

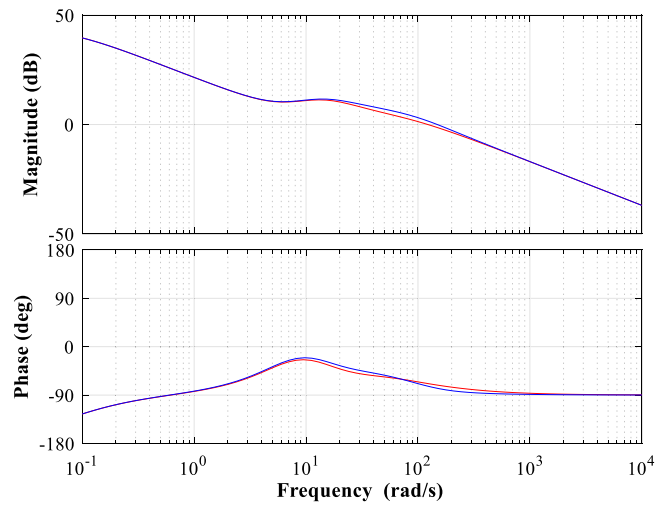


FIGURE 4. Bode plot of open loop transfer function between I_{1q}^* to I_{1q} (red line: voltage drop terms are ignored in the FF current controller, blue line: voltage drop terms are included in the FF current controller, $K_p = \sigma L_1/T_d$, $K_i = R_1/T_d$).

TABLE 1. Configuration of Induction Motor

Symbol	Quantity	Value
R_1	Primary resistance	0.0971 Ω
L_1	Primary self-inductance	30.12 mH
R_2	Secondary resistance	0.0816 Ω
L_2	Secondary self-inductance	29.93 mH
M	Mutual inductance	29.1 mH
σL_1	Primary leakage inductance in FOC	1.83 mH
$\frac{R_2}{L_2}$	Reciprocal of secondary time constant	2.73 (1/s)

$$- \omega_1 \sigma L_1 \frac{1}{1 + sT_d} I_{1q}^* \quad (9)$$

$$V_{1q}^* = \left(K_p + \frac{K_i}{s} \right) (I_{1q}^* - I_{1q}) + R_1 \frac{1}{1 + sT_d} I_{1q}^* + \omega_1 \sigma L_1 \frac{1}{1 + sT_d} I_{1d}^* + \omega_1 \frac{M^2}{L_2} \frac{1}{1 + sT_2} I_{1d}^* \quad (10)$$

where the proportional gain K_p is $\sigma L_1/T_d$ and the integral gain K_i is R_1/T_d . Fig. 4 shows the bode plots of the open loop transfer function between I_{1q}^* and I_{1q} in Fig. 1. Table 1 summarizes the motor parameters used for the calculation in Fig. 4. The d- and q-axis current commands are respectively 93 A and 180 A, the primary angular frequency ω_1 is 63 rad/s, and the time constant of the current controller is 10 ms in this calculation. The red line represents the bode plot that the voltage drop terms in the FF current controller are ignored, and the blue line represents the bode plot that the voltage drop terms are included in the FF current controller in Fig. 4. As a result of Fig. 4, the characteristics of both current controllers are approximately same even if the voltage drop terms are included in the FF current controller.

Therefore, this study assumes that the FF current controller has the voltage drop terms.

B. RELATIONSHIP BETWEEN OUTPUT VOLTAGE OF PI CURRENT CONTROLLER AND MOTOR PARAMETER ERROR

The d- and q-axis output voltage commands V_{1d}^* and V_{1q}^* of the current controller in the steady state are respectively expressed as

$$V_{1d}^* = V_{1dPI} + R_{1s}I_{1d}^* - \omega_1(\sigma L_1)_s I_{1q}^* \quad (11)$$

$$V_{1q}^* = V_{1qPI} + R_{1s}I_{1q}^* + \omega_1(\sigma L_1)_s I_{1d}^* + \left(\frac{M^2}{L_2}\right)_s I_{1d}^* \quad (12)$$

where V_{1dPI} and V_{1qPI} represent the output voltages of the PI current controller; s represents the set value of motor parameters that are not true value in the current controller to define the motor parameter errors. The method that makes the set value to be the true value of the motor parameter is investigated in this study. The mutual inductance $(M^2/L_2)_s$ when the IFOC is realized is given by

$$\left(\frac{M^2}{L_2}\right)_s = L_{1s} - (\sigma L_1)_s \quad (13)$$

The d- and q-axis secondary fluxes Φ_{2d} and Φ_{2q} based on the third and fourth equations in (1) are respectively presented as

$$\Phi_{2d} = \frac{\left(\frac{R_2}{L_2}\right)^2 MI_{1d} + R_2 \frac{M}{L_2} \omega_s^* I_{1q}}{\left(\frac{R_2}{L_2}\right)^2 + \omega_s^{*2}} \quad (14)$$

$$\Phi_{2q} = \frac{\left(\frac{R_2}{L_2}\right)^2 MI_{1q} - R_2 \frac{M}{L_2} \omega_s^* I_{1d}}{\left(\frac{R_2}{L_2}\right)^2 + \omega_s^{*2}} \quad (15)$$

The d- and q-axis motor voltages V_{1d} and V_{1q} are assumed to be equivalent to the d- and q-axis voltage commands V_{1d}^* and V_{1q}^* in the steady state in this section. The d- and q-axis output voltages of the PI current controller according to (3), (4), (11), and (12) are respectively expressed as

$$V_{1dPI} = -(R_{1s} - R_1)I_{1d}^* + \omega_1((\sigma L_1)_s - \sigma L_1)I_{1q}^* - \omega_1 \frac{M}{L_2} \Phi_{2q} \quad (16)$$

$$V_{1qPI} = -(R_{1s} - R_1)I_{1q}^* - \omega_1((\sigma L_1)_s - \sigma L_1)I_{1d}^* - \omega_1 \left(\left(\frac{M^2}{L_2}\right)_s I_{1d}^* - \frac{M}{L_2} \Phi_{2d} \right) \quad (17)$$

The derivatives of the output voltages of the PI current controller with respect to the primary angular frequency are derived from (16) and (17), as shown in

$$\frac{\partial V_{1dPI}}{\partial \omega_1} = ((\sigma L_1)_s - \sigma L_1)I_{1q}^* - \frac{M}{L_2} \Phi_{2q} \quad (18)$$

$$\frac{\partial V_{1qPI}}{\partial \omega_1} = -((\sigma L_1)_s - \sigma L_1)I_{1d}^* - \left(\left(\frac{M^2}{L_2}\right)_s I_{1d}^* - \frac{M}{L_2} \Phi_{2d} \right) \quad (19)$$

Therefore, the primary angular frequency dependency of the output voltage of the PI current controller includes information regarding the motor flux. The relationship between the

derivatives of the output voltages of the PI current controller and the motor parameters based on (2), (13)–(15), (18), and (19) is respectively shown as

$$\frac{\partial V_{1dPI}}{\partial \omega_1} = ((\sigma L_1)_s - \sigma L_1)I_{1q}^* - \frac{M \left(\frac{R_2}{L_2}\right)^2 MI_{1q} - R_2 \frac{M}{L_2} K_s \frac{I_{1q}^*}{I_{1d}^*} I_{1d}}{\left(\frac{R_2}{L_2}\right)^2 + \left(K_s \frac{I_{1q}^*}{I_{1d}^*}\right)^2} \quad (20)$$

$$\frac{\partial V_{1qPI}}{\partial \omega_1} = -(L_{1s} - \sigma L_1)I_{1d}^* + \frac{M \left(\frac{R_2}{L_2}\right)^2 MI_{1d} + R_2 \frac{M}{L_2} K_s \frac{I_{1q}^*}{I_{1d}^*} I_{1q}}{\left(\frac{R_2}{L_2}\right)^2 + \left(K_s \frac{I_{1q}^*}{I_{1d}^*}\right)^2} \quad (21)$$

The motor parameter errors of the current controller are defined as

$$\Delta L_1 = L_{1s} - L_1 \quad (22)$$

$$\Delta K_s = K_s - \frac{R_2}{L_2} \quad (23)$$

$$\Delta(\sigma L_1) = (\sigma L_1)_s - \sigma L_1 \quad (24)$$

The relationship between the derivatives of the output voltages of the PI current controller and motor parameter errors according to (20)–(24) is shown as

$$\frac{\partial V_{1dPI}}{\partial \omega_1} = \Delta(\sigma L_1)I_{1q}^* - \frac{M \left(\frac{R_2}{L_2}\right)^2 MI_{1q} - R_2 \frac{M}{L_2} \left(\Delta K_s + \frac{R_2}{L_2}\right) \frac{I_{1q}^*}{I_{1d}^*} I_{1d}}{\left(\frac{R_2}{L_2}\right)^2 + \left(\left(\Delta K_s + \frac{R_2}{L_2}\right) \frac{I_{1q}^*}{I_{1d}^*}\right)^2} \quad (25)$$

$$\frac{\partial V_{1qPI}}{\partial \omega_1} = -(L_1 + \Delta L_1 - \sigma L_1)I_{1d}^* + \frac{M \left(\frac{R_2}{L_2}\right)^2 MI_{1d} + R_2 \frac{M}{L_2} \left(\Delta K_s + \frac{R_2}{L_2}\right) \frac{I_{1q}^*}{I_{1d}^*} I_{1q}}{\left(\frac{R_2}{L_2}\right)^2 + \left(\left(\Delta K_s + \frac{R_2}{L_2}\right) \frac{I_{1q}^*}{I_{1d}^*}\right)^2} \quad (26)$$

Therefore, the d-axis primary angular frequency dependency of the output voltage of the PI current controller includes the error of the leakage and secondary fluxes; the q-axis dependency includes the error of the primary linkage and secondary fluxes. The derivative of the q-axis output voltage of the PI current controller when the error of primary self-inductance ΔL_1 is zero is expressed as follows based on (26).

$$\frac{\partial V_{1qPI}}{\partial \omega_1}$$

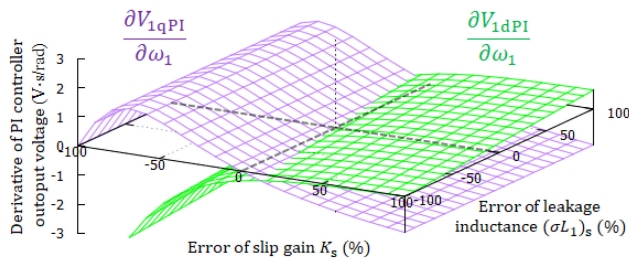


FIGURE 5. Calculated result of derivative of PI current controller output voltage versus error of slip gain K_s and leakage inductance $(\sigma L_1)_s$.

$$= \frac{M}{L_2} \left(-MI_{1d}^* + \frac{\left(\frac{R_2}{L_2}\right)^2 MI_{1d} + R_2 \frac{M}{L_2} \left(\Delta K_s + \frac{R_2}{L_2}\right) \frac{I_{1q}^*}{I_{1d}^*} I_{1q}}{\left(\frac{R_2}{L_2}\right)^2 + \left(\left(\Delta K_s + \frac{R_2}{L_2}\right) \frac{I_{1q}^*}{I_{1d}^*}\right)^2} \right) \quad (27)$$

Therefore, the primary angular frequency dependency of the q-axis output voltage of the PI current controller includes only the error in the secondary flux when the correct primary self-inductance is provided. The error of the secondary flux can be compensated for by adjusting the slip gain to make the derivative of the q-axis output voltage of the PI current controller zero.

The derivative of the d-axis output voltage of the PI current controller when the error of the slip gain is zero is presented below according to (25).

$$\frac{\partial V_{1dPI}}{\partial \omega_1} = \Delta(\sigma L_1) I_{1q}^* \quad (28)$$

Therefore, the primary angular frequency dependency of the d-axis output voltage of the PI current controller includes only the error in the leakage flux when the slip gain has no errors.

Fig. 5 shows the calculation results of the d- and q-axis primary angular frequency dependencies of the output voltage of the PI current controller with respect to the errors of the slip gain and leakage inductance based on (25) and (27). Table 1 summarizes the motor parameters used for the calculations in Fig. 5. In this study, an electric railway vehicle is assumed to be one of the inertial load-drive applications, and therefore, the 150 kW induction motor configuration is used in Table 1. In the IM drive for electric railway vehicles, the operation at the rated point is assumed such that the d- and q-axis current commands are selected to make the torque and flux the rated values, wherein the d-axis current command is 93 A and the q-axis current command is 180 A, as indicated in Fig. 4. The calculation result shown in Fig. 5 indicate that the d- and q-axis angular frequency dependencies of the output voltage of the PI current controller become zero only at the point where both the errors of slip gain and leakage inductance are zero. Hence, the errors of the leakage and secondary fluxes can be compensated by adjusting the slip gain and leakage inductance to make the d- and q-axis derivatives of the output

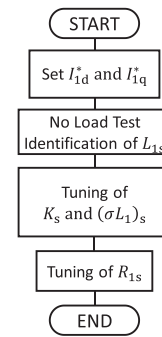


FIGURE 6. Flowchart of proposed auto-tuning.

voltage of the PI current controller zero when the primary self-inductance is given.

C. PROPOSED AUTO-TUNING METHOD

Fig. 6 shows a flowchart of the proposed auto-tuning method. In the proposed method, primary self-inductance is first identified at by the no-load test because it is essential for identifying the slip gain and leakage inductance. When the q-axis current is zero, the motor voltage is presented as

$$V_1 = \sqrt{R_1^2 + (\omega_1 L_1)^2} I_{1d} \quad (29)$$

The voltage drop in the primary resistance is negligible in the high-speed region; the motor voltage is shown as

$$V_1 = \omega_1 L_1 I_{1d} \quad (30)$$

Therefore, the primary self-inductance is identified by the no-load test as

$$L_{1s} = \frac{V_1}{\omega_1 I_{1d}} \quad (31)$$

The estimation error of the primary self-inductance with respect to the primary angular frequency according to (22), (29), and (30) is shown as

$$\Delta L_1 = \frac{\sqrt{R_1^2 + (\omega_1 L_1)^2}}{\omega_1} - L_1 \quad (32)$$

Fig. 7 shows the calculation result of the estimation error of the primary self-inductance with respect to the primary angular frequency according to (32). Table 1 summarizes the motor parameter used for the calculation in Fig. 7. The estimation error of the primary self-inductance is large in the low-speed region. Therefore, the primary self-inductance is identified in the high-speed region.

The slip gain and leakage inductance are identified based on the angular frequency dependencies of the d- and q-axis output voltages of the PI current controller during the acceleration operation. The slip gain is adjusted based on (27) as

$$K_{s_{n+1}} = K_{s_n} + A_{K_s} \frac{\partial V_{1qPI}}{\partial \omega_1} \quad (33)$$

where A_{K_s} represents the correction gain to adjust the slip gain.

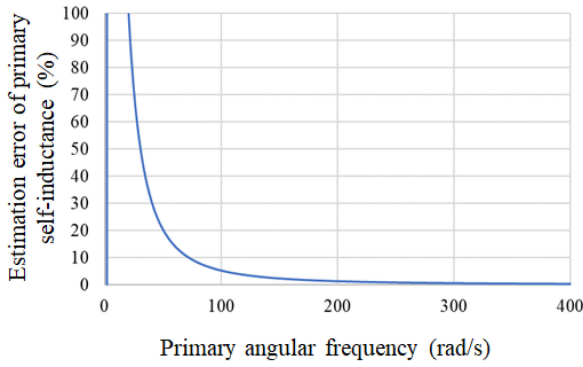


FIGURE 7. Estimation error of primary self-inductance with respect to primary angular frequency.

The leakage inductance is adjusted based on (28) as

$$(\sigma L_1)_{s_{n+1}} = (\sigma L_1)_{s_n} + A_\sigma \frac{\partial V_{1dPI}}{\partial \omega_1} \quad (34)$$

where A_σ represents the correction gain to adjust the leakage inductance.

The angular frequency dependency of the d- and q-axis output voltages of the PI current controller becomes 0 Vs/rad when the slip gain and leakage inductance are identified. The PI current controller compensates for the error in the voltage drops of the primary resistance. Therefore, the primary resistance is identified based on the q-axis output voltage of the PI current controller during the acceleration operation. The error in the primary resistance is defined as

$$\Delta R_1 = R_{1s} - R_1 \quad (35)$$

The q-axis output voltage of the PI current controller after the identification of the slip gain and leakage inductance based on (17) and (35) is given as

$$V_{1qPI} = -\Delta R_1 I_{1q}^* \quad (36)$$

Therefore, the primary resistance is adjusted as

$$R_{1s_{n+1}} = R_{1s_n} + A_R V_{1qPI} \quad (37)$$

where A_R represents the correction gain to adjust the primary resistance. The q-axis output voltage of the PI current controller becomes 0 V when the primary resistance is identified.

III. CONVERGENCE OF AUTO-TUNING AND CALCULATION METHOD FOR CORRECTION GAIN

A. CONVERGENCE OF PROPOSED AUTO-TUNING METHOD

Fig. 8 shows the calculation results of the convergence of the auto-tuning of the slip gain based on (27) and (33). The motor parameters are listed in Table 1. This calculation assumes that the primary self-inductance is provided, and the d- and q-axis currents are equivalent to the d- and q-axis current commands, respectively, where the d-axis current is 93 A and the q-axis current is 180 A. The initial value of the slip gain has an error of 30% with respect to the true value R_2/L_2 . Auto-tuning requires a long time to converge for a small correction gain. The polarity of the slip gain error changes with each tuning

for a large correction gain because the quantity required to compensate for the slip gain is considerably high. Thus, the auto-tuning diverges, as shown in Fig. 8(c).

Fig. 9 shows the calculation results of the auto-tuning of leakage inductance; this calculation is based on (28) and (34). In addition to the calculation conditions shown in Fig. 8, this calculation assumes that the error of the slip gain is 0%, and the initial value of the leakage inductance has an error of 30% with respect to the true value σL_1 . Auto-tuning requires a long time to converge for a small correction gain. The polarity of the leakage inductance error changes with each tuning for a large correction gain because the quantity required to compensate for the leakage inductance is considerably high. Therefore, the auto-tuning diverges, as shown in Fig. 9(c).

Fig. 10 shows the calculation results of the auto-tuning of the primary resistance; this calculation is based on (36) and (37). In addition to the calculation conditions shown in Fig. 9, this calculation assumes that the error in the leakage inductance is 0%, and the initial value of the primary resistance has an error of 30% with respect to the true value R_1 . Auto-tuning requires a long time to converge for a small correction gain. The polarity of the primary resistance error changes with each tuning for a large correction gain because the quantity required to compensate for the primary resistance is considerably high. Therefore, the auto-tuning diverges, as shown in Fig. 10(c).

Hence, the proposed auto-tuning methods require a determination method for the correction gains.

B. CALCULATION METHOD FOR CORRECTION GAIN

The calculation method for the correction gain A_{K_s} is shown based on (27) and (33). However, the analytical solution of the correction gain A_{K_s} with respect to the slip gain error ΔK_s becomes complex because (27) is not linear in the slip gain error ΔK_s . Fig. 11 shows the relationship between (27) and the slip gain error; the calculation conditions are the same as those shown in Fig. 5. Near a 0% slip gain error, the angular frequency dependency of the q-axis output voltage of the PI controller is considered linear with respect to the slip gain error. The Maclaurin expansion of (27) with respect to the slip gain error is presented as

$$\frac{\partial V_{1qPI}}{\partial \omega_1} = -\frac{M^2 I_{1d}^* I_{1q}^{*2}}{R_2 (I_{1d}^{*2} + I_{1q}^{*2})} \Delta K_s \quad (38)$$

The slip gain error is defined again as

$$\Delta K_{s_n} = K_{s_n} - K_{s_{n+1}} \quad (39)$$

Assuming that ΔK_{s_n} is equivalent to ΔK_s , the correction gain A_{K_s} based on (33), (38), and (39) is shown as

$$A_{K_s} = \frac{R_2 (I_{1d}^{*2} + I_{1q}^{*2})}{M^2 I_{1d}^* I_{1q}^{*2}} \quad (40)$$

Thus, the correction gain A_{K_s} is calculated using the initial values of the secondary resistance R_{2s_0} and mutual inductance

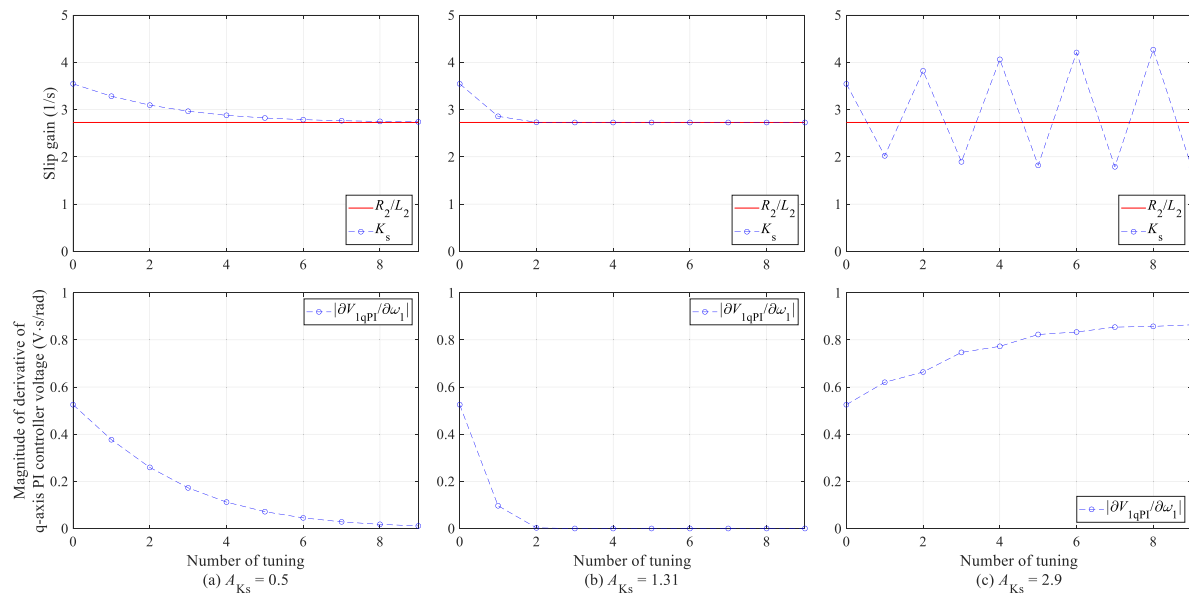


FIGURE 8. Calculated result of the convergence of auto-tuning for slip gain K_s .

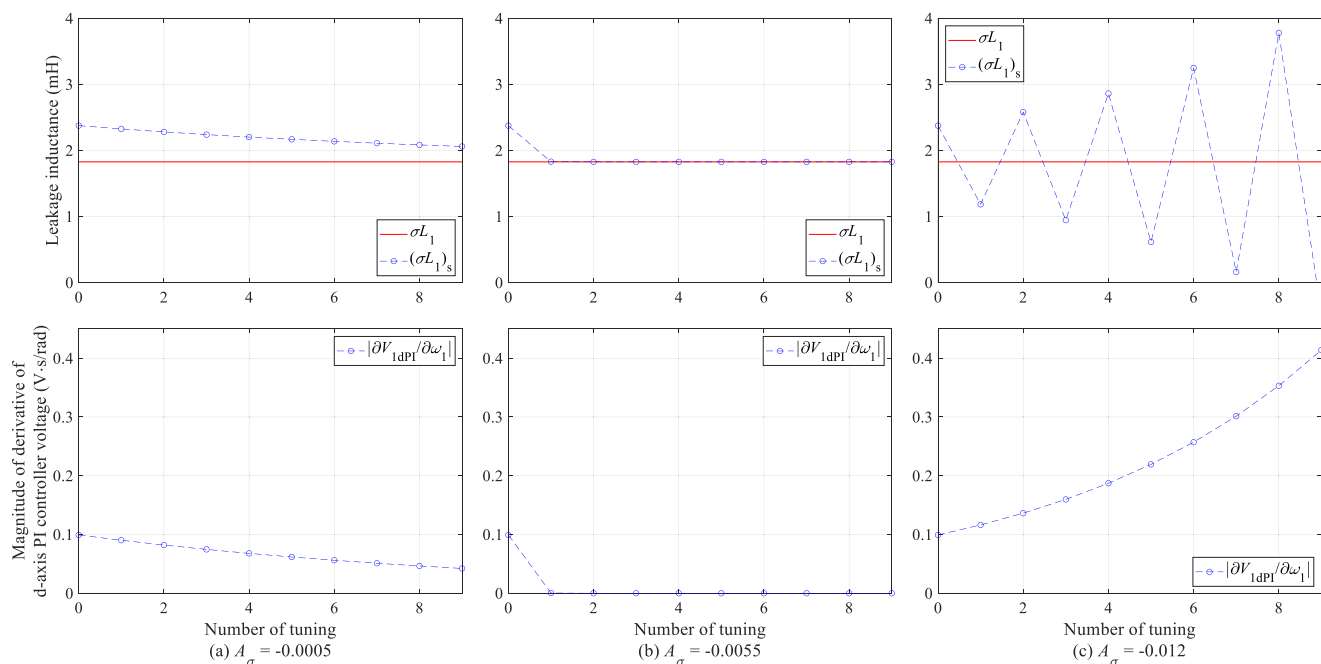


FIGURE 9. Calculated result of the convergence of auto-tuning for leakage inductance $(\sigma L_1)_s$.

M_{s0} before auto-tuning as

$$A_{K_s} = \frac{R_{2s0}(I_{1d}^{*2} + I_{1q}^{*2})}{M_{s0}^2 I_{1d}^* I_{1q}^*} \quad (41)$$

Auto-tuning may diverge when the initial values of the secondary resistance and mutual inductance have large errors with respect to the true values. Convergence of auto-tuning for the slip gain with respect to the initial motor parameter errors is calculated. Errors in the initial secondary resistance

and mutual inductance are defined as

$$\Delta R_2 = R_{2s0} - R_2 \quad (42)$$

$$\Delta M = M_{s0} - M \quad (43)$$

Fig. 12 shows the convergence calculation result of auto-tuning according to (27), (33), (39), and (41)–(43). The motor parameters are listed in Table 1, and the slip gain error ΔK_s is 30%. The d- and q-axis current commands are 93 and 180 A,

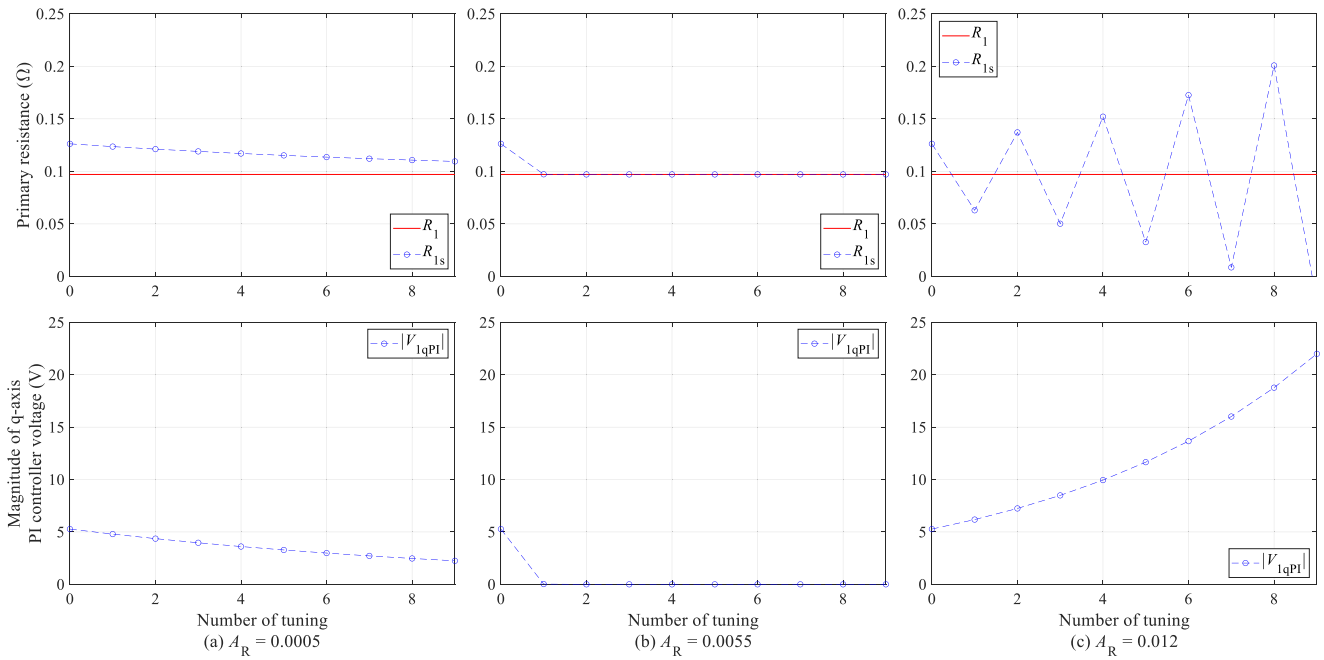


FIGURE 10. Calculated result of the convergence of auto-tuning for primary resistance R_{1s} .

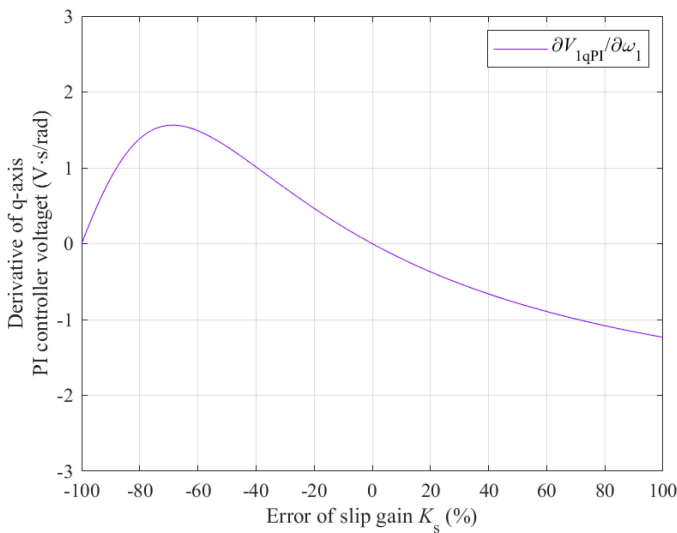


FIGURE 11. Derivative of q-axis PI current controller output voltage versus error of slip gain.

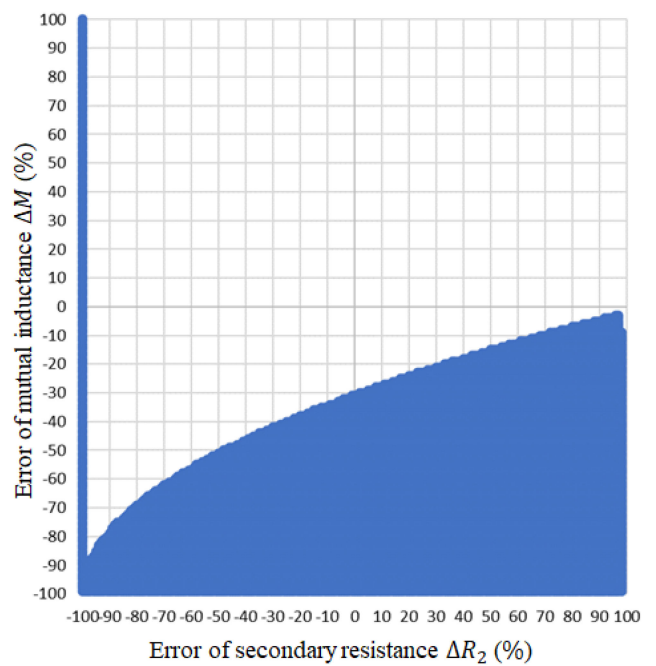


FIGURE 12. Convergence region of auto-tuning for slip gain with respect to initial parameter errors of mutual inductance and secondary resistance (white: converge, blue: not converge).

respectively. The area filled in blue represents the combination of errors ΔR_2 and ΔM where auto-tuning does not converge; here, the secondary resistance error ΔR_2 is -100% , which means that the initial secondary resistance R_{2s0} is $0\ \Omega$, and the motor is not rotated such that auto-tuning does not converge. In the case of a small initial mutual inductance, the correction gain A_{K_s} represented in (41) become too large so that auto-tuning does not converge. Auto-tuning tends to diverge in the case of a large secondary resistance error ΔR_2 because the large secondary resistance makes the correction gain A_{K_s} in (41) larger. The mutual inductance value is approximately

same as the primary self-inductance value; the deviation between the mutual inductance and primary self-inductance is less than 10% . Therefore, auto-tuning converges when the primary self-inductance is identified.

The calculation method for the correction gain A_σ is presented. The angular frequency dependency of the d-axis

output voltage of the PI current controller is linear with respect to the leakage inductance error for a 0% slip gain error, as shown in (28). The leakage inductance error is defined again as

$$\Delta(\sigma L_1)_n = (\sigma L_1)_{s_n} - (\sigma L_1)_{s_{n+1}} \quad (44)$$

Assuming that $\Delta(\sigma L_1)_n$ is equivalent to $\Delta(\sigma L_1)$, the correction gain A_σ is calculated according to (28), (34), and (44) as

$$A_\sigma = -\frac{1}{I_{1q}^*} \quad (45)$$

The q-axis output voltage of the PI current controller is linear with respect to the primary resistance error when slip gain and leakage inductance are identified, as shown in (36). The primary resistance error is defined again as

$$\Delta R_{1n} = R_{1s_n} - R_{1s_{n+1}} \quad (46)$$

Assuming that ΔR_{1n} is equivalent to ΔR_1 , the correction gain A_R is calculated according to (36), (37), and (46) as

$$A_R = \frac{1}{I_{1q}^*} \quad (47)$$

IV. SIMULATION VERIFICATION

A numerical simulation, which assumes a railway vehicle traction system, is conducted to verify whether the proposed methods make parameter identification feasible. The motor parameters are listed in Table 1. Table 2 lists the initial motor parameters of the current controller that have errors with respect to the parameters in Table 1, wherein the motor parameter error is 20% and auto-tuning converges. The correction gains are calculated according to (41), (45), and (47). The DC link voltage is 1500 V, and the d- and q-axis current commands 93 A and 180 A, respectively. In this simulation, the PWM control is not considered because the purpose is verifying the proposed methods in principle. In addition, the integral gain of the PI current controller in the regenerating region is tuned according to the gain determination method in [31] to avoid the current vibration due to unstable eigenvalues (UEVs) of the IFOC in the regeneration operation.

Fig. 13 shows the simulation results of auto-tuning the primary self-inductance. The q-axis current becomes 0 A after the acceleration operation. The d-axis current, primary angular frequency, and voltage command are sampled during coasting in the steady state; the primary self-inductance is calculated based on (31) during the no-load operation.

Fig. 14 shows the simulation results of auto-tuning the slip gain and leakage inductance, wherein the identification result of the primary self-inductance in Fig. 13 is used. Output voltages of the PI current controller are proportional to the primary angular frequency because the PI current controller compensates for the error in the induced electromotive force. The PI current controller voltages and the primary angular frequency are sampled during acceleration operation in the steady state; the slip gain and leakage inductance are adjusted based on (33) and (34) after acceleration operation. The

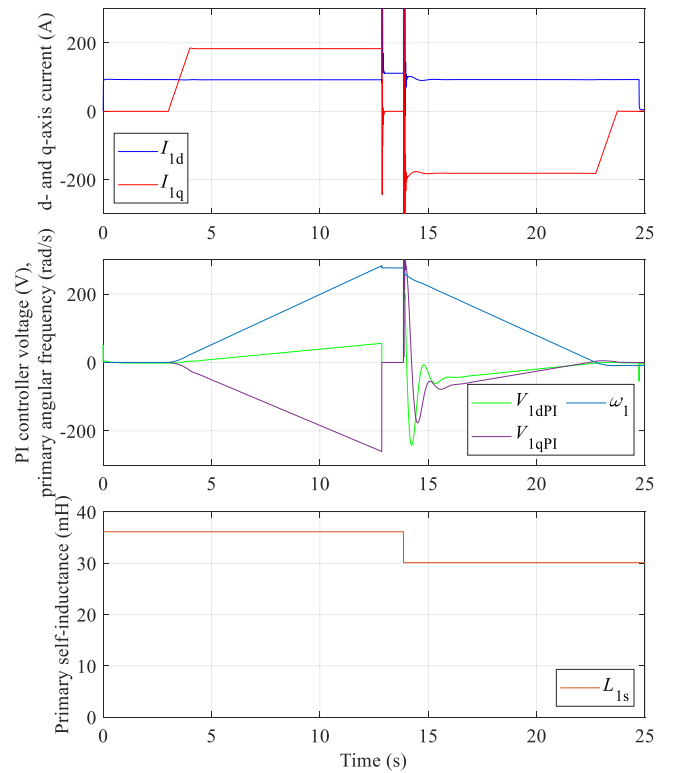


FIGURE 13. Simulation result of auto-tuning for primary self-inductance.

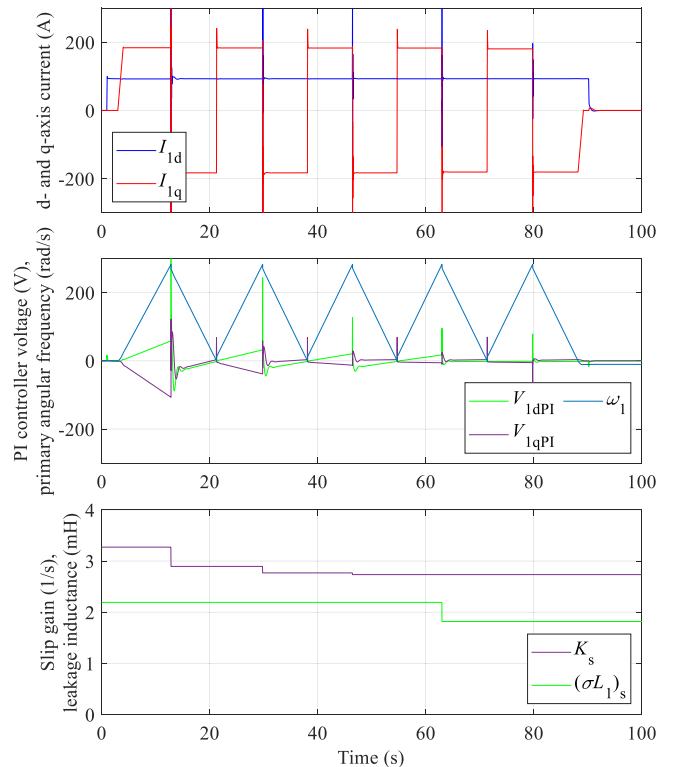


FIGURE 14. Simulation result of auto-tuning for slip gain K_s and leakage inductance $(\sigma L_1)_s$.

TABLE 2. Initial Motor Parameter, Correction Gain, and Adjusted Motor Parameter in Current Controller for Simulation

Symbol	Quantity	Value
R_{1s_0}	Initial set value of primary resistance	0.117 Ω
L_{1s_0}	Initial set value of primary self-inductance	36.14 mH
R_{2s_0}	Initial set value of secondary resistance	0.0979 Ω
L_{2s_0}	Initial set value of secondary self-inductance	37.98 mH
M_{s_0}	Initial set value of mutual inductance	35.91 mH
$(\sigma L_1)_{s_0}$	Initial set value of primary leakage inductance in FOC	2.19 mH
$(M^2/L_2)_{s_0}$	Initial set value of mutual inductance in FOC	33.95 mH
K_{s_0}	Initial set value of slip gain (reciprocal of secondary time constant)	3.27 (1/s)
A_{K_s}	Correction gain for slip gain	1.03
A_σ	Correction gain for leakage inductance	-0.0056
A_R	Correction gain for primary resistance	0.0056
R_{1s}	Adjusted set value of primary resistance	0.0973 Ω
L_{1s}	Adjusted set value of primary self-inductance	30.12 mH
$(\sigma L_1)_s$	Adjusted set value of primary leakage inductance in FOC	1.82 mH
$(M^2/L_2)_s$	Adjusted set value of mutual inductance in FOC	28.3 mH
K_s	Adjusted set value of slip gain (reciprocal of secondary time constant)	2.73 (1/s)

derivative of the output voltage of the PI current controller becomes $0V \cdot s/\text{rad}$ after auto-tuning.

Fig. 15 shows the simulation results of auto-tuning the primary resistance wherein the identification results shown in Figs. 13 and 14 are used. The output voltage of the PI current controller is constant because the controller compensates for the error in the voltage drop of the primary resistance. Further, the q-axis PI current controller voltage is sampled during acceleration operation in the steady state; the primary resistance is adjusted based on (37) after acceleration operation. The output voltage of the PI current controller becomes 0 V after auto-tuning.

Table 2 summarizes the motor parameters after auto-tuning. The motor parameters are identified and compared with Table 1.

V. EXPERIMENTAL RESULT

A. VERIFICATION OF AUTO-TUNING METHOD

Experimental verification is conducted because the dead time of the inverter, forward voltage of the power semiconductor devices, and harmonic components of the current and voltage are not considered in the numerical simulation. An 8-pole 750 W induction motor with an inertial load is used for the

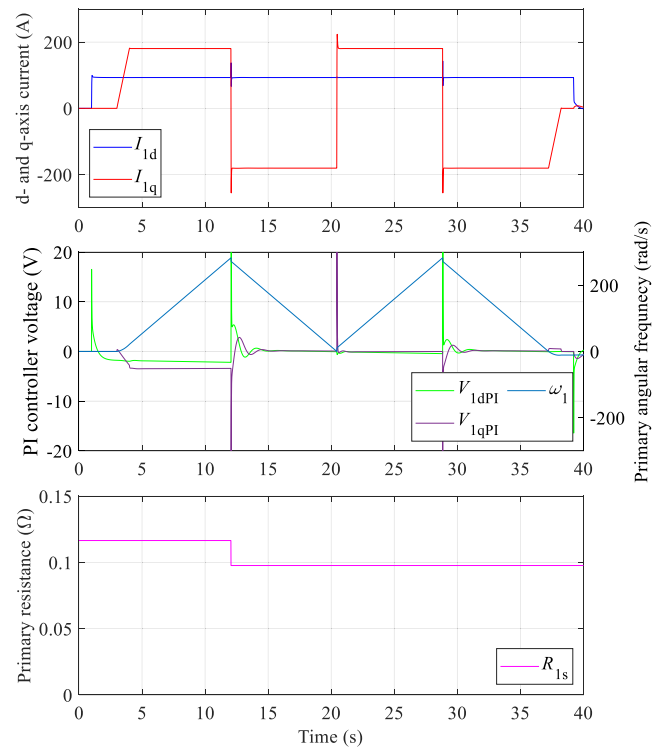


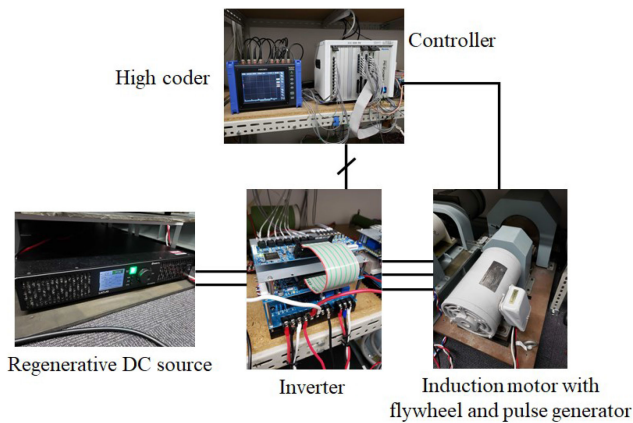
FIGURE 15. Simulation result of auto-tuning for primary resistance R_{1s} .

TABLE 3. Configuration of Induction Motor with Inertia Used for Experimental Verification

Symbol	Quantity	Value
R_1	Primary resistance	3.8 Ω
L_1	Primary self-inductance	112 mH
R_2	Secondary resistance	2.07 Ω
L_2	Secondary self-inductance	123 mH
M	Mutual inductance	100 mH
σL_1	Primary leakage inductance in FOC	31.4 mH
-	Rated output	750 W
-	Poles	8
-	Rated voltage	200 V
-	Rated frequency	50 Hz
-	Rated current	4.80 A
-	Rated speed	700 rpm
-	Total inertia	0.79 $\text{kg} \cdot \text{m}^2$

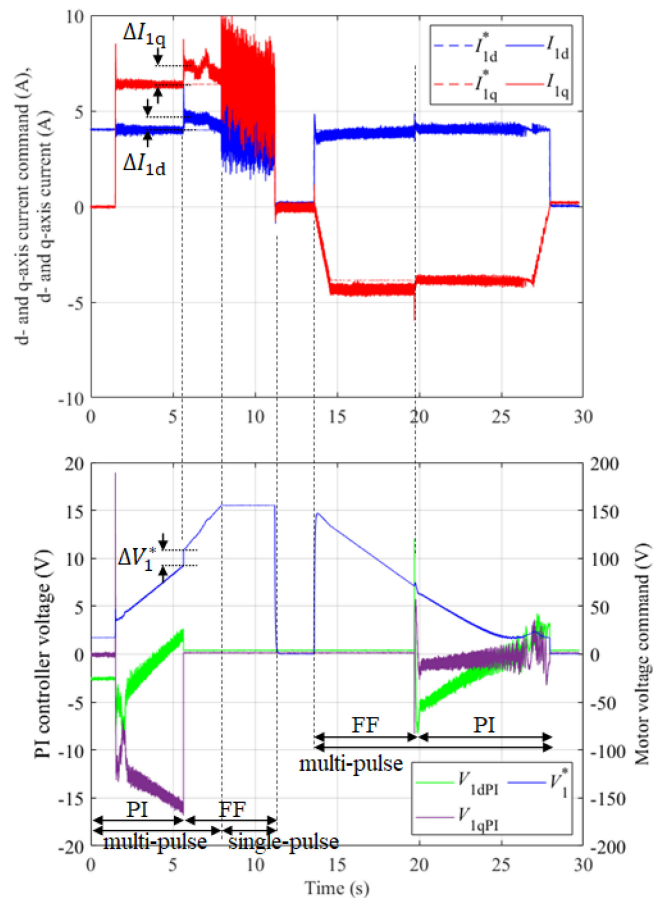
verification. Table 3 summarizes the IM used for the experimental verification. Fig. 16 shows the configuration of the experimental system. Table 4 lists the initial motor parameters and correction gains. The DC link voltage is 200 V, and the d- and q-axis current commands are 4 A and 5.8 A. The current control mode is switched from the PI control mode to the FF control mode at 188 rad/s of the primary angular frequency. The current controller operated at 5 kHz, and the sampling frequency of the auto-tuning controller is 100 Hz.

Fig. 17 shows the experimental waveforms during the acceleration and deceleration operations before auto-tuning. The PI current controller outputs voltages to compensate for the


FIGURE 16. Configuration of experimental system.
TABLE 4. Initial Motor Parameter, Correction Gain, and Adjusted Motor Parameter in Current Controller for Experiment

Symbol	Quantity	Value
R_{1s_0}	Initial set value of primary resistance	5.0 Ω
L_{1s_0}	Initial set value of primary self-inductance	100 mH
R_{2s_0}	Initial set value of secondary resistance	2.9 Ω
L_{2s_0}	Initial set value of secondary self-inductance	125 mH
M_{s_0}	Initial set value of mutual inductance	95.0 mH
$(\sigma L_1)_{s_0}$	Initial set value of primary leakage inductance in FOC	28.0 mH
$(M^2/L_2)_{s_0}$	Initial set value of mutual inductance in FOC	72.0 mH
K_{s_0}	Initial set value of slip gain (reciprocal of secondary time constant)	23.0 (1/s)
A_{K_s}	Correction gain of slip gain	119
A_σ	Correction gain of leakage inductance	-0.172
A_R	Correction gain of primary resistance	0.172
R_{1s}	Adjusted set value of primary resistance	3.6 Ω
L_{1s}	Adjusted set value of primary self-inductance	111 mH
$(\sigma L_1)_s$	Adjusted set value of primary leakage inductance in FOC	31.1 mH
$(M^2/L_2)_s$	Adjusted set value of mutual inductance in FOC	80.1 mH
K_s	Adjusted set value of slip gain (reciprocal of secondary time constant)	16.8 (1/s)

motor parameter errors. The seamless control of currents and voltages is not realized because of the motor parameter errors when the control mode is switched from PI to FF control; the d-axis current deviation ΔI_{1d} between I_{1d}^* and I_{1d} is 0.76 A, the q-axis current deviation ΔI_{1q} between I_{1q}^* and I_{1q} is 1.02 A, and the output voltage deviation ΔV_1^* is 16.8 V in Fig. 17.


FIGURE 17. Experimental result of the acceleration and deceleration operation before auto-tuning.

The d- and q-axis currents are not controlled according to the current commands in the FF control region.

Fig. 18 shows experimental waveforms and motor parameters during auto-tuning. Further, auto-tuning takes approximately 110 s. Fig. 19 shows the experimental waveforms of the auto-tuning of the primary self-inductance. The primary self-inductance is calculated during the no-load operation. Fig. 20 shows the experimental waveforms during the auto-tuning of the slip gain. The slip gain is adjusted based on the primary angular frequency dependency of the q-axis output voltage of the PI current controller during the acceleration operation. The derivative of the q-axis output voltage of the PI current controller becomes 0 V · s/rad in the steady state after the auto-tuning of the slip gain. Fig. 21 shows the experimental waveforms during the auto-tuning of the leakage inductance. The leakage inductance is adjusted based on the primary angular frequency dependency of the d-axis output voltage of the PI current controller during acceleration. The derivative of the d-axis output voltage of the PI current controller becomes 0 V · s/rad in the steady state after the auto-tuning of the leakage inductance. Fig. 22 shows experimental waveforms when auto-tuning the primary resistance. The primary resistance is adjusted based on the q-axis output voltage of the PI current controller during the acceleration

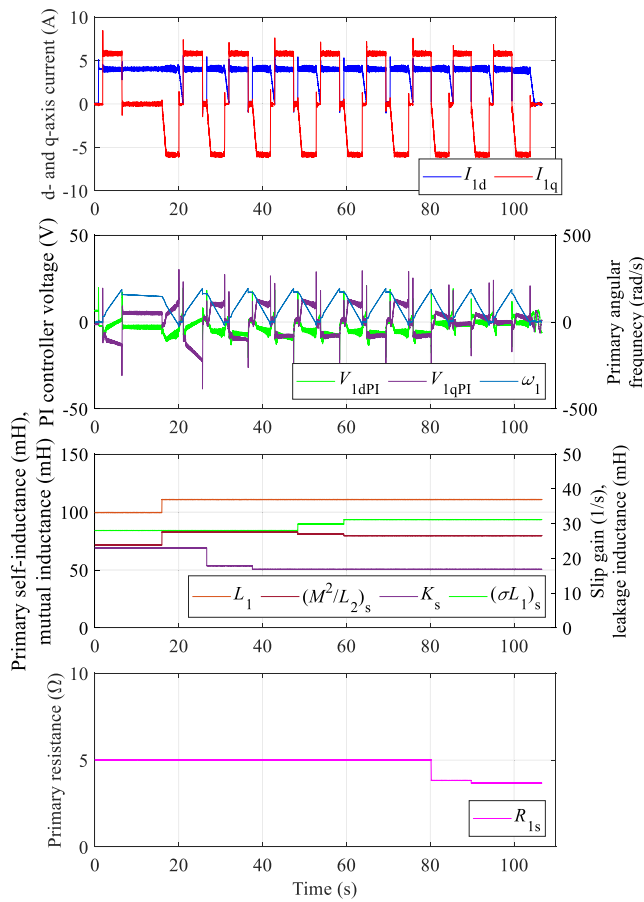


FIGURE 18. Experimental result of auto-tuning.

operation. The output voltage of the PI current controller becomes 0 V in the steady state after auto-tuning.

Table 4 lists the motor parameters after auto-tuning. Fig. 23 shows the experimental waveforms during the acceleration and deceleration operations using the motor parameters listed in Table 4. The seamless control of currents and voltages is realized when the control mode is switched from the PI control to the FF control; the d- and q-axis current deviations and the output voltage deviation are zero. The d- and q-axis currents are controlled based on the current commands in the FF control region.

B. VERIFICATION OF THE CONVERGENCE OF PROPOSED AUTO-TUNING METHOD

The convergence of the proposed auto-tuning and correction gain calculation methods is verified experimentally. Table 5 presents the initial motor parameters. The DC-link voltage is 200 V. The d- and q-axis current commands 4 A and 5.8 A. The experiments are conducted by changing the initial secondary resistance R_{2s0} and mutual inductance M_{s0} according to the flowchart illustrated in Fig. 6. Each initial motor

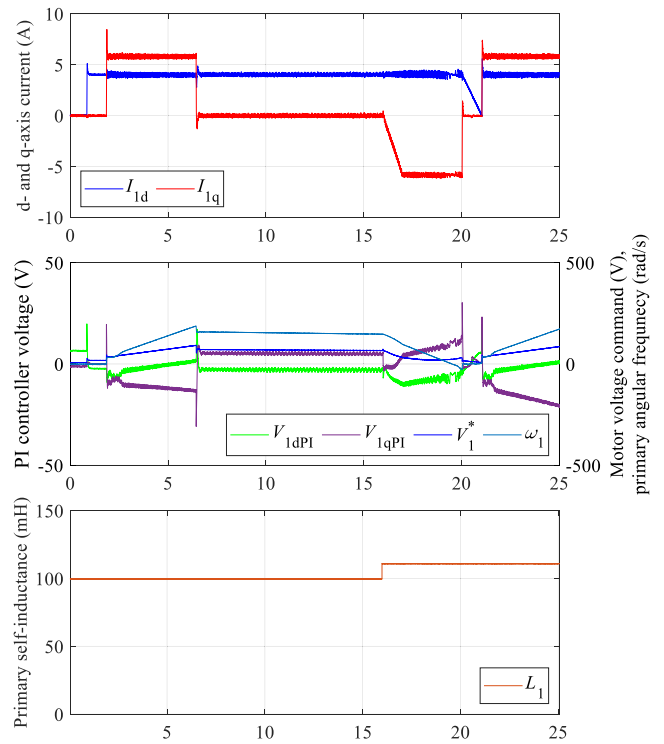


FIGURE 19. Experimental result of auto-tuning for the primary self-inductance L_{1s} .

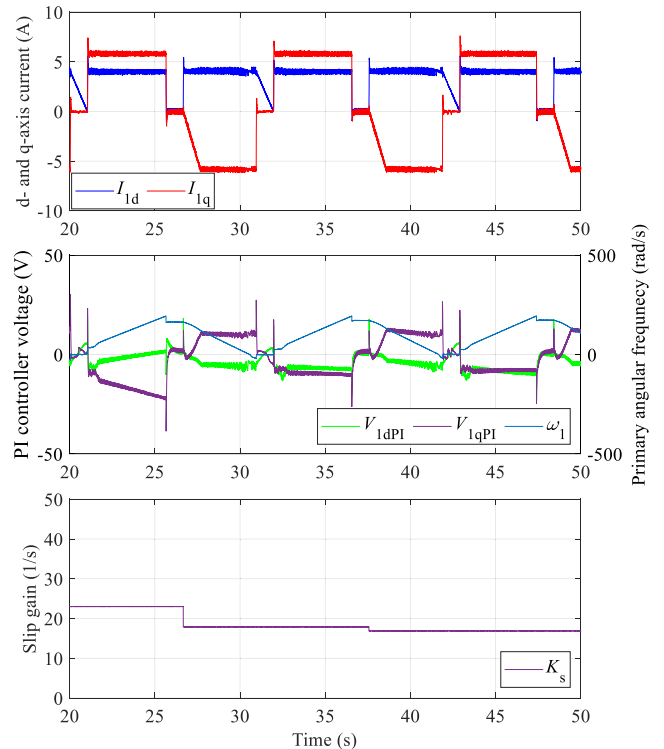


FIGURE 20. Experimental result of auto-tuning for the slip gain K_s .

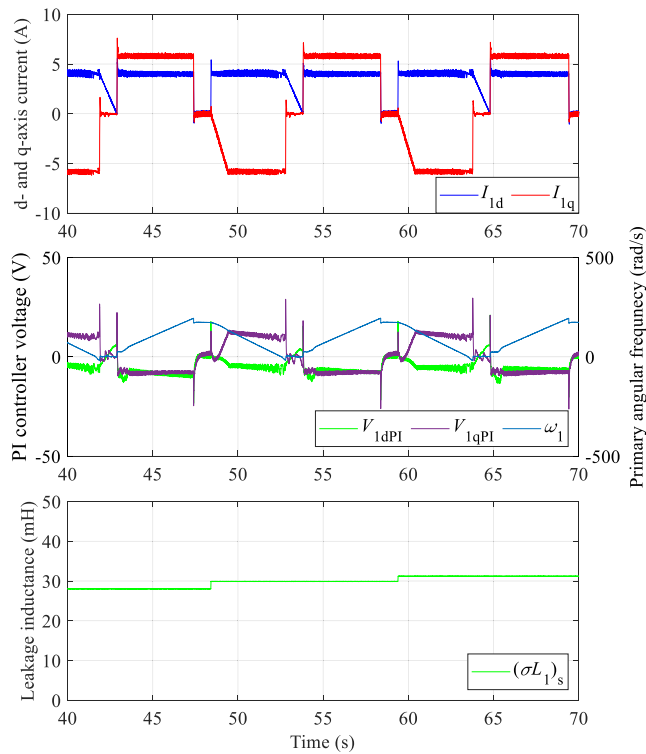


FIGURE 21. Experimental result of auto-tuning for the leakage inductance $(\sigma L_1)_s$.

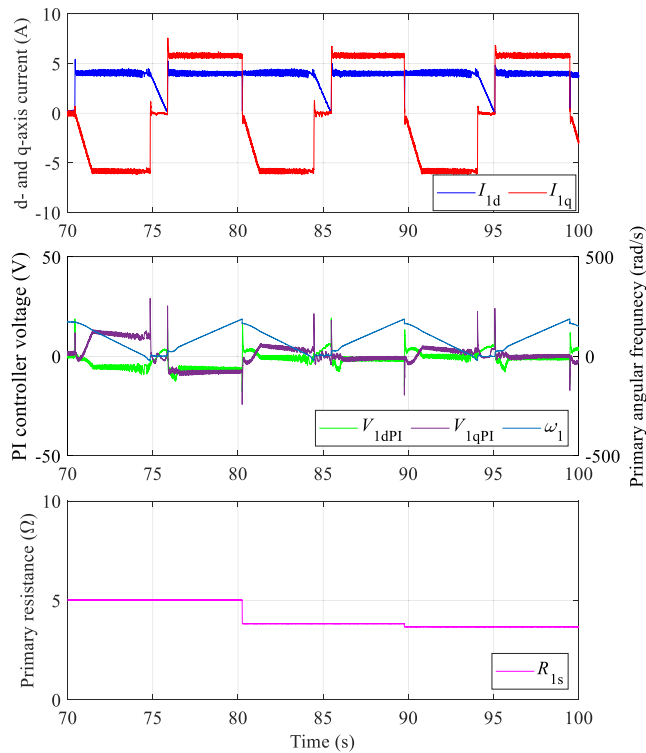


FIGURE 22. Experimental result of auto-tuning for the primary resistance R_{1s} .

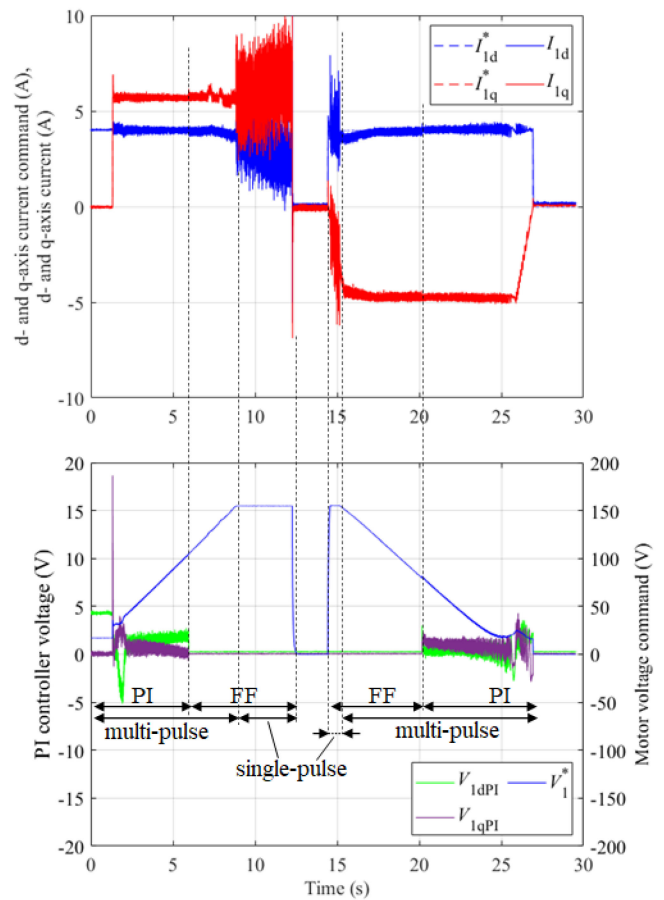


FIGURE 23. Experimental result of the acceleration and deceleration operation after auto-tuning.

TABLE 5. Initial Motor Parameter and Correction Gain for Convergence Verification of Auto-Tuning

Symbol	Quantity	Value
R_{1s_0}	Initial set value of primary resistance	5.0 Ω
L_{1s_0}	Initial set value of primary self-inductance	100 mH
R_{2s_0}	Initial set value of secondary resistance	- Ω
L_{2s_0}	Initial set value of secondary self-inductance	125 mH
M_{s_0}	Initial set value of mutual inductance	- mH
$(\sigma L_1)_{s_0}$	Initial set value of primary leakage inductance in FOC	- mH
$(M^2/L_2)_{s_0}$	Initial set value of mutual inductance in FOC	- mH
K_{s_0}	Initial set value of slip gain (reciprocal of secondary time constant)	- (1/s)
A_{K_s}	Correction gain of slip gain	-
A_{σ}	Correction gain of leakage inductance	- 0.172
A_R	Correction gain of primary resistance	0.172

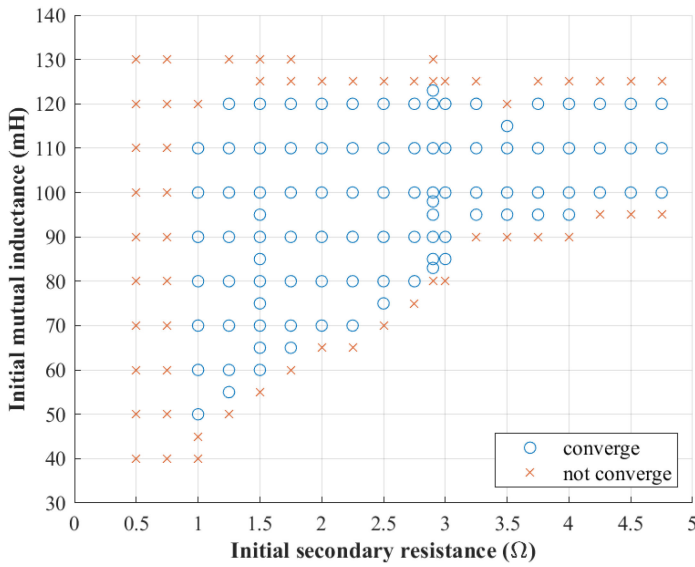


FIGURE 24. Convergence region of auto-tuning with respect to the initial parameter errors of the mutual inductance and secondary resistance.

parameter for the IFOC is defined as

$$\left(\frac{M^2}{L_2}\right)_{s_0} = \frac{M_{s_0}^2}{L_{2s_0}} \quad (48)$$

$$(\sigma L_1)_{s_0} = L_{1s_0} - \left(\frac{M^2}{L_2}\right)_{s_0} \quad (49)$$

$$K_{s_0} = \frac{R_{2s_0}}{L_{2s_0}} \quad (50)$$

The correction gain A_{K_s} is calculated as shown in (41). Fig. 24 shows the verification results of the auto-tuning convergence with respect to the initial secondary resistance and mutual inductance. The motor torque becomes small for a small secondary resistance so that the motor is not accelerated. In this case, it is necessary to increase the secondary resistance or the q-axis current command. The IFOC becomes unstable because the leakage inductance becomes negative for a large mutual inductance, according to (49). This case is negligible because the leakage inductance is defined as a positive value. The auto-tuning does not converge because the correction gain A_{K_s} becomes too large according to (41) for a small mutual inductance, as described in Section III-B. Thus, auto-tuning converges by using the identified primary self-inductance value as the mutual inductance value when calculating the correction gain A_{K_s} .

VI. CONCLUSION

Calculation methods for the correction gains for the proposed auto-tuning method are proposed, and the convergence of the proposed calculation and auto-tuning methods is verified. The motor speed changes gradually in inertial load-drive applications, and therefore, the PI current controller voltage

is proportional to the primary angular frequency and motor parameter errors. Thus, the proposed auto-tuning method identifies motor parameters based on the primary angular frequency dependency of the PI current controller voltage during acceleration with an inertial load. The proposed method is categorized as a method that estimates the motor parameters by changing the frequency or motor speed. Auto-tuning does not converge or takes a long time to converge when correction gains for the proposed methods are inappropriate. Thus, in this study, the calculation methods for the correction gains for auto-tuning are derived from the relationship between the PI current controller voltage, primary angular frequency, and motor parameter errors. The proposed calculation methods for the correction gains are verified by the convergence calculation and experiments. The proposed calculation methods allow the auto-tuning to converge fewer times by using the identified primary self-inductance value as the mutual inductance value when calculating the correction gain A_{K_s} . The acceleration and deceleration operations are seamlessly realized because of the proposed auto-tuning. The sampling frequency of the auto-tuning controller was 100 Hz in the experiments. Therefore, the proposed method can be applied to online auto-tuning for inertial load drive applications with a low-computational-capacity controller.

REFERENCES

- [1] S. M. Tripathi and R. Vaish, "Taxonomic research survey on vector controlled induction motor drives," *IET Power Electron.*, vol. 12, no. 7, pp. 1603–1615, 2019.
- [2] R. Gabriel, W. Leonhard, and C. J. Nordby, "Field-Oriented control of a standard AC motor using microprocessors," *IEEE Trans. Ind. Appl.*, vol. IA-16, no. 2, pp. 186–192, Mar. 1980.
- [3] Y. Sadali *et al.*, "Identifying the optimal induction motor design for increased power density in commuter railway use through loss analysis," in *Proc. 12th Energy Convers. Congr. Expo. - Asia*, 2021, pp. 1187–1192.
- [4] M. Yokoo and K. Kondo, "Damping control of induction motor traction system in single-pulse mode of field weakening region," in *Proc. Int. Conf. Elect. Syst. for Aircr., Railway, Ship Propulsion Road Veh.*, 2015, pp. 1–6.
- [5] R. Krishnan and A. S. Bharadwaj, "A review of parameter sensitivity and adaptation in indirect vector controlled induction motor drive systems," *IEEE Trans. Power Electron.*, vol. 6, no. 4, pp. 695–703, Oct. 1991.
- [6] H. A. Toliyat, E. Levi, and M. Raina, "A review of RFO induction motor parameter estimation techniques," *IEEE Trans. Energy Convers.*, vol. 18, no. 2, pp. 271–283, Jun. 2003.
- [7] S. A. Odhano, P. Pescetto, H. A. A. Awan, M. Hinkkanen, G. Pellegrino, and R. Bojoi, "Parameter identification and self-commissioning in AC motor drives: A technology status review," *IEEE Trans. Power Electron.*, vol. 34, no. 4, pp. 3603–3614, Apr. 2019.
- [8] T. Matsuo and A. Lipo, "A rotor parameter identification scheme for vector-controlled induction motor drives," *IEEE Trans. Ind. Appl.*, vol. IA-21, no. 3, pp. 624–632, May 1985.
- [9] C. M. Verrelli, A. Savoia, M. Mengoni, R. Marino, P. Tomei, and L. Zarri, "On-Line identification of winding resistances and load torque in induction machines," *IEEE Trans. Control Syst. Technol.*, vol. 22, no. 4, pp. 1629–1637, Jul. 2014.
- [10] F. Lin and H. Su, "A high-performance induction motor drive with On-line rotor time-constant estimation," *IEEE Trans. Energy Convers.*, vol. 12, no. 4, pp. 297–303, Dec. 1997.
- [11] R. F. F. Koning, C. T. Chou, M. H. G. Verhaegen, J. B. Klaassens, and J. R. Uittenbogaart, "A novel approach on parameter identification for inverter driven induction machines," *IEEE Trans. Control Syst. Technol.*, vol. 8, no. 6, pp. 873–882, Nov. 2000.

- [12] K. Wang, J. Chiasson, M. Bodson, and L. M. Tolbert, "A nonlinear least-squares approach for identification of the induction motor parameters," *IEEE Trans. Autom. Control*, vol. 50, no. 10, pp. 1622–1628, Oct. 2005.
- [13] K. Wang, J. Chiasson, M. Bodson, and L. M. Tolbert, "An online rotor time constant estimator for the induction machine," *IEEE Trans. Control Syst. Technol.*, vol. 15, no. 2, pp. 339–348, Mar. 2007.
- [14] M. H. Shin and D. S. Hyun, "Online identification of stator transient inductance in rotor-flux-oriented induction motor drive," *IEEE Trans. Ind. Electron.*, vol. 54, no. 4, pp. 2018–2023, Aug. 2007.
- [15] W. M. Lin, T. J. Su, and R. C. Wu, "Parameter identification of induction machine with a starting no-load low-voltage test," *IEEE Trans. Ind. Electron.*, vol. 59, no. 1, pp. 352–360, Jan. 2012.
- [16] Y. He, U. Wang, Y. Feng, and Z. Wang, "Parameter identification of an induction machine at standstill using the vector constructing method," *IEEE Trans. Power Electron.*, vol. 27, no. 2, pp. 905–915, Feb. 2012.
- [17] S. R. P. Reddy and U. Loganathan, "Offline recursive identification of electrical parameters of VSI-fed induction motor drives," *IEEE Trans. Power Electron.*, vol. 35, no. 10, pp. 10711–10719, Oct. 2020.
- [18] H. Zhao et al., "Parameter identification based online noninvasive estimation of rotor temperature in induction motors," *IEEE Trans. Ind. Appl.*, vol. 57, no. 1, pp. 417–426, Jan./Feb. 2021.
- [19] M. Akiyama, K. Kobayashi, I. Miki, and M. A. El-Sharkawi, "Auto-tuning method for vector controlled induction motor drives," *IEEJ Trans.*, vol. 116-D, no. 8, pp. 844–851, 1996.
- [20] M. W. Degner, J. M. Guerrero, and F. Briz, "Slip-Gain estimation in field-orientation-controlled induction machines using the system transient response," *IEEE Trans. Ind. Appl.*, vol. 42, no. 3, pp. 702–711, May/June 2006.
- [21] D. Perdukova, P. Palacky, P. Fedor, P. Bober, and V. Fedak, "Dynamic identification of rotor magnetic flux, torque and rotor resistance of induction motor," *IEEE Access*, vol. 8, pp. 142003–142015, 2020.
- [22] F. Erturk and B. Akin, "A robust method for induction motor magnetizing curve identification at standstill," *IEEE Access*, vol. 7, pp. 55422–55431, 2019.
- [23] H. Sugimoto and S. Tamai, "Secondary resistance identification of an induction-motor applied model reference adaptive system and its characteristics," *IEEE Trans. Ind. Appl.*, vol. 1A-23, no. 2, pp. 296–303, Mar. 1987.
- [24] J. K. Seok, S. H. Moon, and S. K. Sul, "Induction machine parameter identification using PWM inverter at standstill," *IEEE Trans. Energy Conv.*, vol. 12, no. 2, pp. 127–132, Jun. 1997.
- [25] M. Carraro and M. Zigliotto, "Automatic parameter identification of inverter-fed induction motors at standstill," *IEEE Trans. Ind. Electron.*, vol. 61, no. 9, pp. 4605–4613, Sep. 2014.
- [26] Y. S. Kwon, J. H. Lee, S. H. Moon, B. K. Kwon, C. H. Choi, and J. K. Seok, "Standstill parameter identification of vector-controlled induction motors using the frequency characteristics of rotor bars," *IEEE Trans. Ind. Appl.*, vol. 45, no. 5, pp. 1610–1618, Sep./Oct. 2009.
- [27] M. Ranta and M. Hinkkanen, "Online identification of parameters defining the saturation characteristics of induction machines," *IEEE Trans. Ind. Appl.*, vol. 49, no. 5, pp. 2136–2145, Sep./Oct. 2013.
- [28] T. Kobayashi, Y. Kimpara, M. Fukuda, and T. Onuma, "Motor constants measurement for induction motors without rotating," *IEEJ Trans. Ind. Appl.*, vol. 128, no. 1, pp. 18–26, 2008.
- [29] J. Y. Ruan and S. M. Wang, "Magnetizing curve estimation of induction motors in single-phase magnetization mode considering differential inductance effect," *IEEE Trans. Power Electron.*, vol. 31, no. 1, pp. 497–506, Jan. 2016.
- [30] M. Nagataki, K. Kondo, O. Yamazaki, K. Yuki, and Y. Nakazawa, "Auto tuning method to identify motor stator and rotor parameter in field-orientation-controlled induction motor," in *Proc. IEEE Energy Convers. Congr. Expo.*, 2020, pp. 5805–5812.
- [31] M. Nagataki, K. Kondo, O. Yamazaki, K. Yuki, and Y. Nakazawa, "Regenerating-Mode stabilization of indirect-field-orientation-controlled induction motor for inertial load drive," in *Proc. IEEE Energy Convers. Congr. Expo.*, 2021, pp. 4908–4914.

MASAKI NAGATAKI (Member, IEEE) received the M. Eng. degree from the Graduate School of Science and Engineering, Chiba University, Chiba, Japan, in 2020. He is currently working toward the Ph.D. degree with the Graduate School of Advanced Science Engineering, Waseda University, Tokyo, Japan. His research interests include power electronics and motor-drive.

KEIICHIRO KONDO (Member, IEEE) received B.S. and Dr. Eng. degrees from the Faculty of Electrical Engineering, Waseda University, Tokyo, Japan, in 1991 and 2000, respectively. From 1991 to 2006, he was a Senior Researcher with Rolling Stock Control Division, Railway Technical Research Institute, Tokyo, Japan. From 2007 to 2018, he was with Electrical and Electronic Engineering Course of Graduate School, Chiba University, Chiba, Japan. Since 2018, he has been a Professor with the School of Advance Science and Engineering, Department of Electrical Engineering and Bio Science, Waseda University. His research interests include power electronics, AC motor drive, energy storage system, wireless power transmission, and their application to the railway vehicle traction and electric vehicles.

He is a Senior Member of the Institute of Electrical Engineers of Japan (IEEJ).

OSAMU YAMAZAKI received the B. Eng. degree from the Faculty of Electrical Engineering, Yamagata University, Yamagata, Japan, in 1993. Since 1993, he has been with Toshiba Infrastructure Systems and Solutions Co. Ltd., Kanagawa, Japan.

KAZUAKI YUKI received the M. Eng. degree from Graduate School of Electrical Engineering, Keio University, Tokyo, Japan, in 1994. From 1994, he has been with Toshiba Infrastructure Systems and Solutions Co. Ltd., Kanagawa, Japan.

YOSUKE NAKAZAWA received the M. Eng. degree from Department of Electrical Engineering and Information Systems, Graduate School of Engineering, The University of Tokyo, Tokyo, Japan, in 1991.

Since 1991, he has been with Toshiba Infrastructure Systems and Solutions Co. Ltd., Kanagawa, Japan.